Energy & Buildings 323 (2024) 114772

Contents lists available at ScienceDirect

Energy & Buildings

journal homepage: www.elsevier.com/locate/enbuild

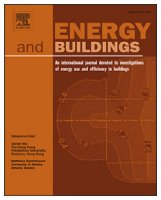

Dynamic grid emission factors and export limits reduce emission abatement and cost benefits of building PV systems

Linda Brodnicke [a,1], Alissa Ganter [a,1], Sven Tröber [a,b], Giovanni Sansavini [a], Natasa Vulic [b,*]

[a] Institute of Energy and Process Engineering, ETH Zürich, Zürich, Switzerland
[b] Laboratory for Urban Energy Systems, Empa, Dübendorf, Switzerland

ARTICLE INFO

Keywords:
PV system design
Multi-objective optimization
GHG abatement
Self-sufficiency
Self-consumption

ABSTRACT

Photovoltaic (PV) installations in the building sector are expected to play a crucial role in Switzerland's efforts to achieve decarbonization targets. Nevertheless, most analyses on PV system design prioritize economic factors, and overlook the impact of angle-dependent PV generation, dynamic grid greenhouse gas (GHG) emissions, and export limitations on their emission abatement potential during operation. Our study sheds light on the cost- and emission-optimal orientation and sizing of PV systems in buildings, factoring in hourly grid GHG emission intensity and curtailment measures. We employ mixed-integer linear programming (MILP) and illustrate the methodology for a case study building under different scenarios, aiming to minimize costs and emissions by considering a combination of rooftop and façade PV systems, and a battery. We show that assuming a constant annual grid GHG emission intensity may overestimate annual emission abatement potential of PV generation by a factor of two, emphasizing the need for dynamic grid GHG emission intensity. When considered, cost-optimal solutions favour larger systems that maximize total production. In contrast, emission-optimal solutions increase self-consumption via inclusion of battery systems. Curtailment due to export limitations reduces the cost and emission benefits of excess generation (from feed-in tariff payments and carbon credits), prompting a trend towards smaller PV installations with steeper panel tilts. Thus, the emission abatement potential of PV generation heavily depends on the option to export excess electricity production.

1. Introduction

1.1. Motivation

In alignment with the Paris Agreement, Switzerland aims to reach net-zero greenhouse gas (GHG) emissions by 2050 [1]. The emission reduction strategy includes increasing the penetration of variable renewable generation, mainly from solar photovoltaic (PV), while simultaneously phasing out nuclear power plants. As a result, increased dependence on electricity imports is expected during winter [2].

Due to land constraints, new PV installations are expected to evolve primarily in the building sector. For instance, the Energy Perspectives for Switzerland exclusively consider the use of available rooftop and façade areas in their PV expansion projections to meet 34TWh [2], about half of the estimated potential from rooftop and façade PV systems [3]. In 2022, the majority of capacity was installed on residential buildings, followed by the industry, trade, and service sectors; less than 10% of the capacity involved utility-scale systems (larger than 1MW) [4]. Consequently, ensuring optimal economic and environmental benefits of building PV systems is essential in reaching decarbonization targets. The GHG emission intensity of grid electricity plays a crucial role for quantifying the GHG emissions abatement of PV stemming from self-consumption and surplus generation. To this aim, the large hourly and seasonal fluctuations of the GHG emission intensity of the electric grid must be accounted for [5,6]. In particular, a reduction of GHG emissions-intensive winter electricity imports would contribute significantly to the net-zero strategy [7]. As neighbouring countries also pursue decarbonization, Swiss electricity import patterns will be affected by coinciding generation deficits in winter and surpluses in summer [8]. Moreover, large expansion of decentralized export from PV generation is expected to lead to curtailment of locally produced PV electricity due to local network constraints [9–11]. To reduce grid expansion costs, moderate export limits have already been implemented in some regions. For

* Corresponding author.
E-mail address: natasa.vulic@empa.ch (N. Vulic).
[1] Authors contributed equally.

https://doi.org/10.1016/j.enbuild.2024.114772
Received 17 December 2023; Received in revised form 11 July 2024; Accepted 4 September 2024
Available online 10 September 2024

Table 1
Building level studies on optimal PV placement.

Source	Main decision variables	Objectives
Litjens et al. [15]	rooftop PV tilt and azimuth	self-consumption, revenue
Rowlands et al. [17]	rooftop PV tilt and azimuth	revenue
Brito et al. [16]	rooftop and façade PV area (fixed orientation)	payback time
Lovati et al. [18]	rooftop and façade PV area (fixed orientation)	net present value
Weniger et al. [21]	rooftop PV tilt and azimuth	self-sufficiency, cost
Azzoli et al. [23]	rooftop PV tilt and azimuth	curtailment
Matthis et al. [24]	rooftop PV tilt and azimuth	curtailment
Laveyne et al. [25]	rooftop PV tilt and azimuth	congestion, over-voltage
Waibel et al. [26]	rooftop and façade PV area (fixed orientation)	cost, emissions

instance, the German Renewable Energy act (EEG) has stipulated an export limit corresponding to 70% of rated DC power of the installed PV system [12]. Distribution system operators in Switzerland are proposing a similar approach. Due to ease of implementation, they propose placing fixed export limits of 70% for smaller, building system installations (30 kVA or less) without compensation [13]. Moreover, static export limits are already common practice in Australia, where under certain conditions, even a zero export limit can be imposed on PV system owners by the grid operators [14]. With increased PV shares, export constraints may become more prevalent in the future. If the locally produced electricity exceeds the export limit and cannot be stored or used locally, the electricity production must be reduced, i.e. curtailed. Consequently, curtailment decreases the potential environmental and economic benefits of PV generation compared to the unconstrained case.

Both time-varying GHG emissions and curtailment influence cost and emission benefits of PV systems during operation. When considered in the design stage, these factors are expected to have a strong impact on the optimal PV system design. As a result, both time-resolved GHG emissions and curtailment must be considered for guiding PV system design in terms of panel area, tilt, and azimuth, as well as the inclusion of a battery system, leading to trade-offs between economic and environmental considerations. This is especially relevant for PV systems in the building sector—both building-applied and building-integrated—due to the constraints of the low-voltage grid where higher rates of curtailment are expected.

1.2. Literature review

Most research on the optimal installation decisions for PV systems focuses either on economic aspects [15–18], the impact on the self-sufficiency and self-consumption [15,19–22] or on curtailment [23–25]. However, the combined consideration of optimal PV area and orientation for time-dependent, i.e. dynamic, grid GHG emission intensities is limited. Table 1 provides a concise overview of studies addressing optimal placement of building PV systems, together with the corresponding decision variables and objectives they considered. Detailed discussions of these studies follow below.

Litjens et al. and Rowlands et al. investigate the optimal PV placement maximizing system revenues. While Litjens et al. observe large variations in the optimal PV orientation for different demand patterns and market prices in Germany and the Netherlands [15], the results from Rowlands et al. indicate that system designs with tilts less than latitude and near south azimuths are optimal across all considered pricing regimes in Ontario, Canada [17]. In this context, Rowlands et al. highlight the importance of further investigating the optimal PV orientation across different geographical locations with improved data availability, and derive general conclusions that can be used to support policy discussions on the implementation of larger PV capacities. Besides rooftop PV, Brito et al. also consider the installation of façade PV, demonstrating its potential to cover mid-day electricity demands in winter and morning/afternoon demands in summer at the cost of longer payback times compared to rooftop installations alone [16]. Moreover, Lovati et al. find that installing PV modules on façades can be economically advantageous due to better load matching in winter [18]. In particular, the inclusion of a battery storage can lead to a higher net present value (NPV) for the PV system, which is, however, often not large enough to offset battery costs. Conversely, Waibel et al. find façade PV beneficial from an environmental perspective but more cost-intensive than battery storage. However, their analysis did not consider embodied emissions, and roof PV installation angles were not optimized but fixed to coincide with the flat roof.

Furthermore, the impact of PV tilt and azimuth angles on self-sufficiency has been analyzed, and Weniger et al. show that when a fixed-capacity battery is included, PV orientation has no major impact on the resulting self-sufficiency. Nevertheless, current favourable feed-in tariffs and high battery costs can lead to larger PV systems without batteries as the cost-optimal solution, while in the long term (assuming both feed-in tariffs and cost of batteries decreases), smaller PV systems with battery and, therefore, increased self-consumption, become the lowest cost solution [21].

In addition, Azzolini et al. analyze the impact of the choice of PV orientation on their curtailment and demonstrate that over- or under-tilting PV panels only has small impacts on their curtailment (<0.06%), and mostly depends on whether the load is dominant in summer or winter [23]. Matthis et al. support this finding, indicating that especially in combination with battery storage capacities, curtailment reduces significantly (<1%) [24]. Finally, the effect of PV panel orientation on congestion and voltage profile is analyzed. In this context, Laveyne et al. show that in local low-voltage grids, the highest curtailed energy occurs for tilts and orientations with the highest annual yield, where curtailment is triggered to avoid over-voltages [25].

To the authors' knowledge, little work has been performed considering the minimization of both emissions and costs, while optimizing PV placement (area, tilt, and orientation) and battery storage for a dynamic grid GHG emission intensity and export limitations.

1.3. This work

In this study, we develop a methodology to evaluate the cost- and emission-optimal placement of rooftop and façade PV systems considering dynamic grid GHG emissions intensities and export limitations. We employ a mixed-integer linear programming (MILP) model to determine the optimal area, tilt, and azimuth of the PV systems, and the optimal storage capacity of the battery system. The input parameters of the optimization problem are time-varying grid GHG emissions, embodied GHG emissions, local electricity prices and feed-in tariffs, and area-dependent PV costs, allowing us to assess the trade-offs between the optimal PV placement and battery storage. The approach is applied to a case study—a multi-storey, mixed-use building [27]—subject to different scenarios of grid GHG emission intensity and export limitation levels, which are implemented as caps on the system's export capacity.

Section 2 outlines the methodology, case study, and scenarios, followed by the presentation and discussion of results in Sec. 3. Section 4 summarizes the key findings.

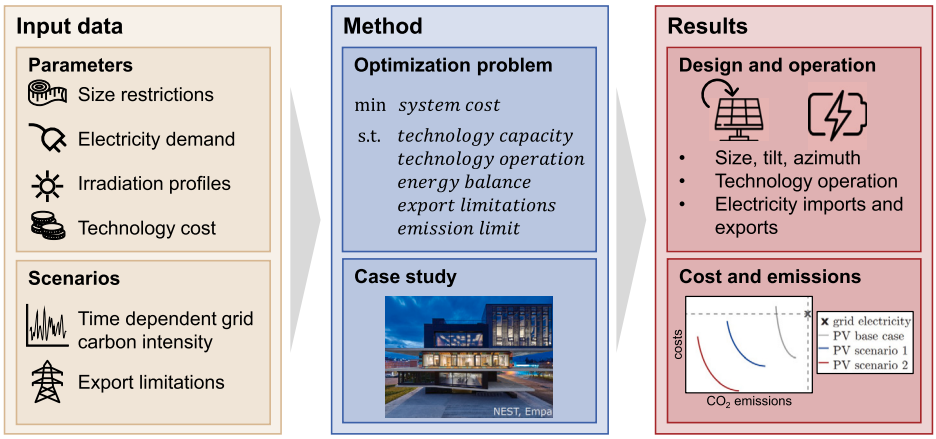

Fig. 1. Illustration of the methodology. An optimization problem is formulated and applied to the case study of the NEST building in Switzerland and the cost-emissions Pareto front is examined for multiple scenarios.

2. Methods

Fig. 1 outlines the methodology, including the input data (technology and case study parameters), the optimization problem, and the results. The optimization considers the costs and emissions associated with the technologies (PV systems and batteries) and the grid electricity as input data (see Sec. 2.1). The case study building provides constraints on the available installation area that can be exploited for capturing the solar resource, calculated for different panel tilts and orientations using weather station measurements [28] and the pvlib library [29]. Further details on the input data and the case study are provided in Sec. 2.1.1. Based on the input data, cost- and emission-optimal solutions are evaluated, and the corresponding installation decisions are assessed under different grid GHG emissions intensities and export limitation scenarios described in Sec. 2.3.

2.1. Optimization formulation

The environmental and economic assessment of the combined PV-plus-storage installation is performed using a MILP optimization problem to determine the optimal system design and operation for the time horizon of one year. The optimization problem is formulated in Python using cvxpy 1.2.0 [30,31] and solved with Gurobi 9.5.1 [32]. The optimization model determines the optimal panel area and orientation (defined by tilt and azimuth angles) that meets the building demand for electricity, heating, and cooling. Both the total annual cost (capital and operational) and total annual GHG emissions (embodied and operational) are minimized. The bi-objective optimization problem is solved using the ϵ-constraint method (see Sec. 2.1.4).

2.1.1. Input data and case study description

Case study overview We consider the NEST living lab, a grid-connected, mixed-used building located in Dübendorf near Zürich, Switzerland [27]. The building configuration present at the end of 2018 is assumed. Office space accounts for around 80% of the total floor area, with residential covering the remaining 20%. In this study, the geometry of the NEST building envelope is simplified by assuming perfectly perpendicular façades throughout the entire height. Shading from surrounding trees or buildings is not considered, which may overestimate the PV generation potential, especially on façades.

Technology characteristics The model optimizes the design and operation of rooftop and façade PV panels and a battery. Other components such as an inverter are not modelled and could be included in future work. The input parameters that describe the modelled PV system and the battery system are reported in Tables 2 and 3, respectively. We assume that crystalline silicon (c-Si) technology is used for rooftop installations, whereas façade panels feature a thin film technology based on copper indium selenide (CIS) solar cells. The assumed efficiency and embodied emissions for each panel type are based on this technology choice. Moreover, a piecewise affine approximation with four segments was used to model the façade and rooftop PV costs based on data from the EnergieSchweiz Solarrechner [33] (see Appendix A.2 for a detailed description). Given the assumption that façade PV systems are building-integrated, the investment cost of BIPV is adjusted by the costs associated with competing conventional building envelope materials that they replace. As a result, a unit cost of 250 CHF/m^2 is deducted from the PV façade cost curves [34,35]. The annuity factors for PV a_{PV} and battery systems a_{BS} are calculated assuming a discount rate of 6% and lifetimes of 30 and 10 years, respectively. Degradation effects are not considered.

PV area and angle limitations For the roof installation, the maximum area is estimated as 880 m^2, which corresponds to 70% of the rooftop area [49]. For the façade, the maximum area is estimated as 350 m^2 per installation, which is equal to 50% of the available area. The reduced available area on the façades compared to the rooftop is due to the assumption that windows make up at least 30% of the façade surface [50]. For the flat rooftop considered here, the angles of the PV panels are defined in 5-degree steps for both the tilt (ranging from 0 to 45°) and the azimuth (ranging from 90 to 270°). For the façade, the angles are fixed to the available south, west, and east orientations, as depicted in Table 4. In the following, the sets $\mathcal{I}$ and $\mathcal{J}$ are used to describe the possible values of the tilt and azimuth angle, respectively.

Electricity imports and exports Both the price at which electricity is purchased from the grid $p_{\mathrm{purchase},t}$ and the price at which PV-generated electricity is sold $p_{\mathrm{FIT},t}$ are based on the pricing scheme of the local electricity provider for the year 2021 [51] (see Appendix A.3). These prices are the end-consumer prices for businesses, and thus include network tariffs, taxes, and levies. In some scenarios, the electricity export capacity is limited to a maximum value P_{Cap}. For a description of the export capacity limitations, the reader is referred to section 2.3. The GHG emissions of the electricity grid are obtained from Rüdisüli et al. [6] and are calculated using a marginal approach with an hourly resolution for the year 2018. To ensure consistency, the building electricity demands and weather data are chosen for the same year, as discussed in more detail below. For the no-nuclear GHG emissions sensitivity analysis scenario, the marginal emissions without the presence of nuclear energy within Switzerland are assumed (see Appendix B for more details).

Building energy demands The measured energy demands for electricity, heating, and cooling for the year 2018 are obtained from the NEST living

Table 2
Technology characteristics of the PV system. The assumed lifetime corresponds to the manufacturer performance guarantee.

	Symbol	PV system	Reference
Capital cost of roof PV	$C_{\text{PV\_roof}}$	area-dependent (see Table A.2)	[33–35]
Capital cost of façade PV	$C_{\text{PV\_facades},k}$	area-dependent (see Table A.2)	[33–35]
Efficiency rooftop	$\alpha_{\text{PV\_roof},i,j,t}$	time- and angle-dependent	-
Efficiency façade	$\alpha_{\text{PV\_facades},k,t}$	time-dependent	-
Nominal PV efficiency rooftop	$\alpha_{\text{PV\_roof}}$	0.2	[36]
Nominal PV efficiency façade	$\alpha_{\text{PV\_facades}}$	0.15	[36]
Heat transfer coefficient rooftop	$U_{\text{c\_roof}}$	20 W/m^{2}K	[37]
Heat transfer coefficient façade	$U_{\text{c\_facades}}$	15 W/m^{2}K	[37]
Absorption coefficient solar irradiance	ß	0.9	[37]
Temperature coefficient rooftop	$\gamma_{\text{PV\_roof}}$	0.45%/°C	[38]
Temperature coefficient façade	$\gamma_{\text{PV\_facades}}$	0.36%/°C	[38]
Embodied emissions rooftop	$e_{\text{PV\_roof}}$	8.3 kg_{GHG}/m^{2}year	[39], [40]
Embodied emissions façade	$e_{\text{PV\_facades}}$	5.3 kg_{GHG}/m^{2}year	[39], [40]
Lifetime	-	30 years	[41,42]

Table 3
Technology characteristics of the battery system.

	Symbol	Battery system	Reference
Unit capital cost	c_{BS}	740 CHF/kWh	[43]
Charging efficiency	η_{c}	0.9	[43]
Discharging efficiency	η_{d}	0.9	[43]
Embodied emissions	e_{BS}	10.4 kg_{GHG}/kWhyear	[44]
Lifetime	-	10 years	[43]
Self discharge rate	λ_{L}	10^{-4} h^{-1}	[45,46]
Minimum SOC	SOC_{min}	0.1	[47,48]
Maximum SOC	SOC_{max}	0.9	[47,48]
Power to energy ratio	-	$\frac{1}{4\text{ h}}$	[43]

Table 4
Technology parameters.

	PV Roof	PV East	PV South	PV West	Battery system
Tilt, i (°)	[0, 45]	90	90	90	-
Azimuth, j (°)	[90, 270]	118	208	298	-
min. Size	0 m^2	0 m^2	0 m^2	0 m^2	0 kWh
max. Size	880 m^2	350 m^2	350 m^2	350 m^2	500 kWh

lab. Thermal demands for both heating and cooling are satisfied by a heat pump system. All energy demand data are preprocessed according to the procedure described in Appendix A.1 and aggregated as electricity demands. An overview of the considered building units, their relative floor areas and annual demands are included in Table A.1.

Rooftop PV: solar radiation and self-shading The solar irradiance is obtained from measured data of the local Meteoswiss weather station [28] for 2018. The measured irradiance data include the global horizontal irradiance (GHI) and diffuse horizontal irradiance (DHI), while the direct normal irradiance (DNI) is estimated based on the sun's position and the two measured irradiance components. Total in-plane irradiance for each considered panel tilt angle i and azimuth angle j is then calculated using the pvlib [29] tool, taking into account all three irradinance components (GHI, DHI, and DNI) and the sun's position. The Perez diffuse irradiance model for tilted surfaces is assumed [52,53]. The resulting matrix $I_{\text{PV\_roof},i,j,t}$ includes the irradiance profiles for all combinations of tilt and azimuth angle that could be installed for the rooftop PV system.

Additionally, inter-row spacing to minimize self-shading is considered when determining the maximum panel area for each tilt i and azimuth angle j. The minimum row spacing is calculated based on sun's position during winter solstice (21st December) between 10 am and 2 pm. The panels are assumed to be arranged in a landscape configuration, with a panel width of 1 meter. The maximum rooftop panel area $A_{\text{PV\_roof,max},i,j}$ therefore depends on the selected tilt and azimuth angles. Specifically, with increasing tilt angles, the spacing between PV panels has to be increased to minimize inter-row shading. The ground coverage ratio (GCR) varies from 1 for the 0 degree tilt to 0.36 for a 45 degree tilt. In other words, the maximum rooftop panel area for panels at 45 degree tilt is only 36% of that for a 0 degree tilt. As a result, a 0 degree panel tilt allows for the largest available installation area, resulting in a maximum electricity output across all seasons (see Fig. 2). While some self-shading may still occur, its effects are not considered in the operation of the system due to the limitations of the simple efficiency model used here.

Façade PV: solar radiation Similarly, the plane-of-array irradiance profiles for the three orientations $I_{\text{PV\_facades},k,t}$ are calculated using the pvlib tool [29], where the façade orientation k indicates whether the façade is south-facing, west-facing, or east-facing. The set $\mathcal{K}$ includes the three directions, and the tilt and azimuth angles are listed in Table 4.

PV efficiency The temperature of PV modules greatly impacts their efficiency [54], leading to a reduction in PV system generation potential. To estimate the combined impact of ambient temperature and solar radiation on the solar cell temperature, several temperature models commonly used in industry and research were considered [55,56]. In this study, we employ the PVSyst temperature cell model [37], an empirical heat loss model, as implemented in the pvlib library [57]. A part of a widely used photovoltaic simulation software, this model was chosen due to the availability of proposed heat loss factors for different mounting modes of the modules that occur in the building sector: fully-insulated backside (representative of facade systems) and semi-integration (representative of roof-mounted systems).

The calculations account for the differences in solar cell technologies (c-Si for the rooftop panels and CIS for the façade panels), the mounting mode (building-applied for rooftop panels and building-integrated for façade PV), and the plane-of-array irradiance that varies with PV orientation. Hence, the resulting PV efficiency is separately calculated for each installation site.

The cell temperature $T_{\text{cell},i,j,t}$ is calculated as:

$$T_{\text{cell},i,j,t} = T_{\text{amb},t} + \frac{1}{U_{\text{c}}}\left(\beta G_{\text{inc},i,j,t}\right)\left(1 - \alpha_{\text{PV}}\right) \tag{1}$$

where $T_{\text{amb},t}$ is the ambient air temperature, U_{c} is the heat transfer coefficient for the respective mounting modes, β is the absorption coefficient of solar irradiance, $G_{\text{inc},i,j,t}$ is the global irradiance for a given azimuth and tilt angle, and α_{PV} is the nominal PV efficiency for the corresponding panel types. Thus, the time-dependent efficiency of the rooftop PV panels is calculated as [58]:

$$\alpha_{\text{PV},i,j,t} = \alpha_{\text{PV}}\left(1 + \gamma_{\text{PV}}(T_{\text{cell},i,j,t} - 25)\right) \tag{2}$$

where γ is the temperature coefficient for the specific type of panel and i, j are the tilt and azimuth angle combinations. Moreover, for each fa-

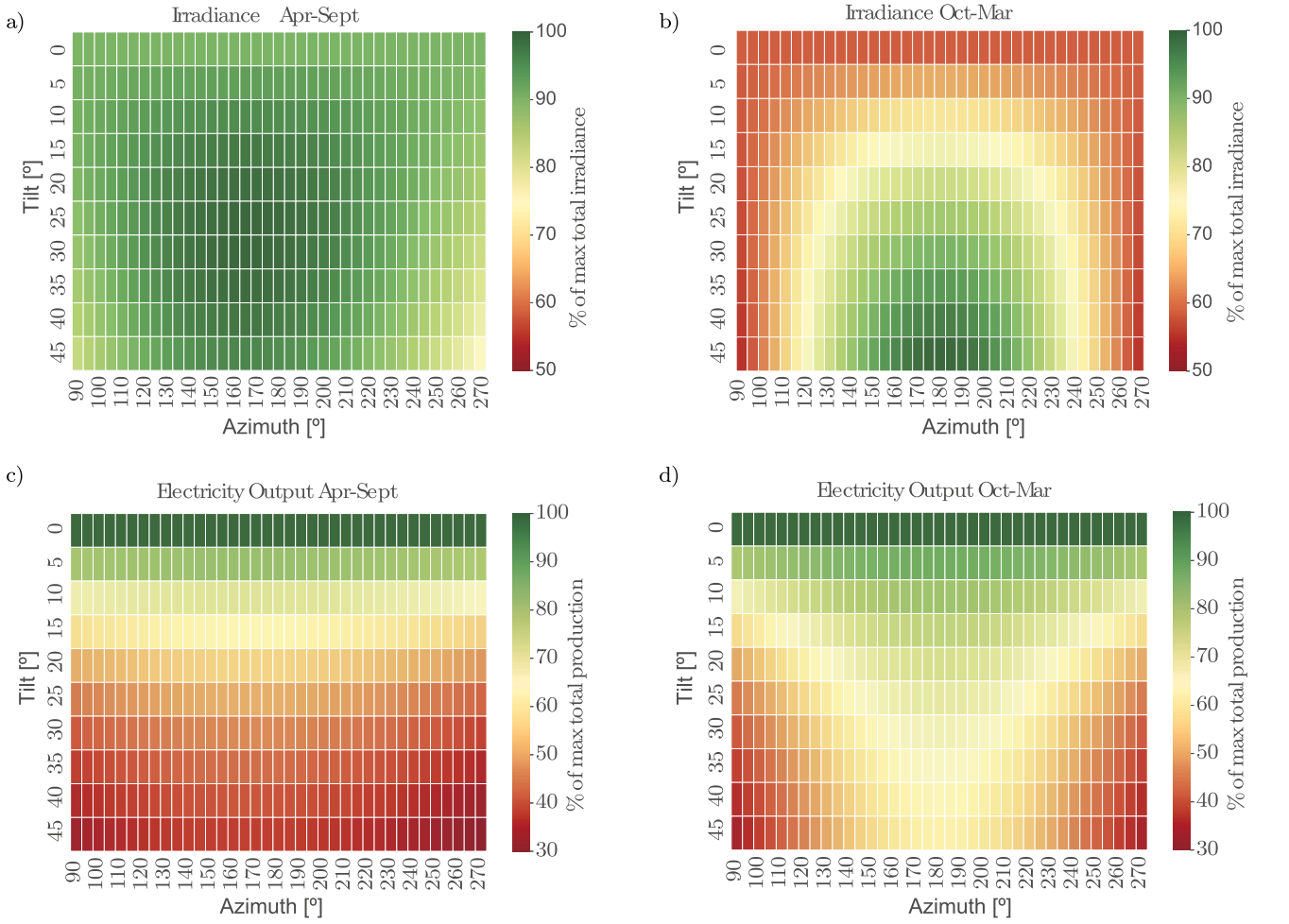

Fig. 2. Irradiance and electricity output during the summer and winter half-year of 2018 for the case study location (Dübendorf, Switzerland). The incident irradiance is higher on surfaces with greater tilts (>30°) in the winter half-year (b), while the maximum total electricity production is highest at a zero degree tilt (d). This effect emerges due to the increased row-spacing between PV panels to minimize self-shading as the tilt of the panels increases. (For interpretation of the colours in the figure(s), the reader is referred to the web version of this article.)

cade orientation k the time-dependent efficiency profiles $\alpha_{\text{PV\_facades},k,t}$ are determined using the information on façade orientation listed in Table 4. System losses, such as soiling, shading, mismatch, wiring, and inverter losses are not explicitly considered in our model. A choice of conservative PV module efficiencies, however, ensures that the power output computed by the model would be comparable to other simple efficiency models that assume higher module efficiencies.

2.1.2. Decision variables

The decision variables of the MILP model include:

- the area of the PV panels on the roof $A_{\text{PV\_roof}}$ and on the façades $A_{\text{PV\_facades},k}$
- the capacity of the battery system $E_{\text{BS,rated}}$
- the orientation of rooftop PV panels $b_{i,j}$ with tilt angle i and azimuth angle j
- the electricity production of the PV panels $P_{\text{PV\_production},t}$ at each timestep $t \in \mathcal{T}$, comprising the electricity production from the rooftop panels $P_{\text{PV\_production\_roof},t}$ and from the façades $P_{\text{PV\_production\_facades},k,t}$
- the electricity curtailment of the PV panels $P_{\text{curtailed},t}$ at each timestep $t \in \mathcal{T}$
- the battery charge $P_{\text{BS\_in},t}$ and discharge $P_{\text{BS\_out},t}$ at each timestep $t \in \mathcal{T}$
- the electricity exported to the grid $P_{\text{grid\_out},t}$ at each timestep $t \in \mathcal{T}$
- the electricity imported from the grid $P_{\text{grid\_in},t}$ at each timestep $t \in \mathcal{T}$

All decision variables are defined as positive real numbers ($\mathbb{R}_0^+$). Decision variables are values the MILP model optimizes for a given objective function whilst adhering to the dependencies included via the constraints.

2.1.3. Objective functions

The cost objective function f_{cost} comprises the annualized capital investment costs f_{cap}, as well as grid electricity imports $f_{\text{op\_cost}}$ and exports $f_{\text{op\_revenue}}$ for all time steps $t \in \mathcal{T}$:

$$f_{\text{cost}} = f_{\text{cap}} + f_{\text{op\_cost}} - f_{\text{op\_revenue}} \tag{3}$$

with

$$f_{cap} = C_{\text{PV\_roof}}\, a_{\text{PV}} + \sum_{k \in \mathcal{K}} C_{\text{PV\_facades},k}\, a_{\text{PV}} + E_{\text{rated,BS}}\, c_{\text{BS}}\, a_{\text{BS}} \tag{4a}$$

$$f_{\text{op\_cost}} = \sum_{t \in \mathcal{T}} p_{\text{purchase},t}\, P_{\text{grid\_in},t} \tag{4b}$$

$$f_{\text{op\_revenue}} = \sum_{t \in \mathcal{T}} p_{\text{FIT},t}\, P_{\text{grid\_out},t} \tag{4c}$$

where $C_{\text{PV\_roof}}$ and $C_{\text{PV\_facade},k}$ describe the area-dependent investment costs for rooftop and façade PV installations, respectively, which

are determined using the piecewise-affine approximation described in Appendix A.2; c_{BS} describes the unit investment costs of the battery systems, and $p_{purchase,t}$ and $p_{FIT,t}$ describe the electricity price and the feed-in tariff (FIT) at time step t, respectively. Thus, the financial benefits from exporting electricity are included via the reimbursement of electricity exports, and the financial benefits from self-consumption are modelled via reduced electricity import costs. Operational and maintenance costs (O&M) associated with the PV and battery systems are not considered.

The GHG emissions objective function f_{GHG} comprises the embodied and operational GHG emissions, $f_{GHG,embodied}$ and $f_{GHG,operation}$, respectively. Electricity exported to the grid provides an emission benefit in the form of GHG emissions credits:

$$f_{GHG} = f_{GHG,embodied} + f_{GHG,operation} \tag{5}$$

with

$$f_{GHG,embodied} = A_{PV\_roof} e_{PV\_roof} + \sum_{k \in \mathcal{K}} A_{PV\_facades} e_{PV\_facades} + E_{BS,rated}\, e_{BS} \tag{6a}$$

$$f_{GHG,operation} = \sum_{t \in \mathcal{T}} m_t \left(P_{grid\_in,t} - P_{grid\_out,t} \right) \tag{6b}$$

where e_{PV_roof} and $e_{PV\_facades}$ are the unit embodied GHG emissions of the rooftop and façade PV panels, respectively. Moreover, e_{BS} is the unit embodied GHG emissions of the battery system, and m_t is the GHG emission intensity of the electricity grid at an hourly resolution. We assume that electricity exports are rewarded with GHG emissions credit benefits, proportional to the marginal grid GHG emission intensity at the time of the export. Thus, environmental benefits from electricity exports are considered via GHG emissions credit benefits, and environmental benefits from self-consumption are considered via a reduction of the emissions associated with electricity imports.

In the operational GHG emission objective (Eq. (6b)), GHG emission benefits correspond to negative operational GHG emissions when electricity is exported to the grid, and serves to offset GHG emissions associated with the imports from the grid. In a simple case of constant GHG emissions ($m_t = C$), this objective would be negative over the full year if the total exports to the grid exceed total imports from the grid. However, when GHG emissions are dynamic, this is not necessarily the case and strongly depends on the relative GHG emission intensities during import and export.

We apply the ϵ-constraint method to solve the bi-objective optimization problem and determine the cost-emissions Pareto front, which describes the set of non-dominated solutions [59]. First, we determine the cost-minimal solution $f_{GHG,min}$ and compute the resulting emissions $f_{GHG,max}$. Thereafter, we determine the emissions-minimal solution $f_{GHG,min}$. Next, we determine the cost-minimal solutions for six fixed emission values within the emissions interval $\left[f_{GHG,min}, f_{GHG,max}\right]$:

$$\text{minimize } f_{cost} \tag{7a}$$

$$\text{subject to } f_{GHG} \leq f_{GHG,min} + \frac{\epsilon_i}{6} \left(f_{GHG,max} - f_{GHG,min} \right) \quad \forall \quad \epsilon_i = \{0, \ldots, 6\} \tag{7b}$$

Note that the cost minimization is still subject to all other constraints introduced in section 2.1.4. The ϵ-constraint method merely introduces an additional constraint.

2.1.4. Constraints

The energy balance ensures that the electricity demand is satisfied at every timestep:

$$P_{demand,t} = P_{PV\_production,t} - P_{BS\_in,t} + P_{BS\_out,t} + P_{grid\_in,t} - P_{grid\_out,t} - P_{curtailed,t} \tag{8}$$

The battery storage can only be used to balance the electricity demand of the case study building and cannot be used for grid arbitrage. Thus, the battery discharge and grid imports are limited by the demand at that time. Furthermore, the local electricity production from PV limits the combined battery charging power and grid exports:

$$P_{BS\_out,t} + P_{grid\_in,t} \leq P_{demand,t} \tag{9a}$$

$$P_{BS\_in,t} + P_{grid\_out,t} \leq P_{PV\_production,t} \tag{9b}$$

In some scenarios, the export capacity is limited to a maximum capacity (for a description, see section 2.3):

$$P_{grid\_out,t} \leq P_{Cap} \tag{10}$$

This export limitation is an absolute value, i.e. the exports are limited to a certain peak power. An alternative way of modelling peak power limitations would be a relative export limitation, where the maximum exports must not exceed a certain fraction of the installed peak capacity. We consider an absolute limitation most suitable to assess the potential of using PV orientation to shift electricity production intra-daily and seasonally, since a relative definition of the export limit would penalize PV orientations that maximize the PV output. In other words, installations with a high specific yield (measured in kWh/kWp) would be more likely to have their energy curtailed under a relative export limit (i.e. relative to their kWp installed).

The overall electricity production from the PV panels at each time step is the sum of the production from the three façade orientations and the rooftop PV panel at this time step:

$$P_{PV\_production,t} = \sum_{k \in \mathcal{K}} P_{PV\_production\_facades,k,t} + P_{PV\_production\_roof,t} \tag{11}$$

To ensure that only electricity produced from the PV panels can be curtailed, the curtailed electricity must not exceed the electricity produced from the PV panels at that time step:

$$P_{curtailed,t} \leq P_{PV\_production,t} \tag{12}$$

The electricity production from each PV façade orientation k depends on the efficiency profile $\alpha_{PV\_facades,k,t}$, the selected panel area $A_{PV\_facades,k}$ and the irradiance profile $I_{PV\_facades,k,t}$. The PV panel area $A_{PV\_facades,k}$ is limited by the maximum PV-panel area $A_{PV\_facades,max,k}$ (Eq. (13)):

$$P_{PV\_production\_facades,k,t} = A_{PV\_facades,k} I_{PV\_facades,k,t} \alpha_{PV\_facades,k,t} \tag{13a}$$

$$A_{PV\_facades,k} \leq A_{PV\_facades,max,k} \tag{13b}$$

The electricity production from rooftop panels depends on the selected tilt angle i and azimuth angle j, and the corresponding irradiance profile $I_{PV\_roof,i,j,t}$, efficiency $\alpha_{PV\_roof,i,j,t}$, as well as the panel area A_{PV_roof}. The selection of the tilt and azimuth angle is modelled with the binary decision variable $b_{i,j}$ and the auxiliary variable for the rooftop PV panel area $\tilde{A}_{i,j}$. If the PV panel with tilt angle i and azimuth angle j is selected, $b_{i,j} = 1$ and the rooftop PV panel area is limited by the maximum PV panel area $\tilde{A}_{i,j} \leq A_{PV\_roof,max,i,j} 1$. Otherwise $b_{i,j} = 0$ and consequently $\tilde{A}_{i,j} = A_{PV\_roof,max,i,j} 0$ (Eqs. 14a–c). Finally, Eq. (14d) ensures that only one combination is selected:

$$P_{PV\_production\_roof,t} = \sum_{i \in \mathcal{I}} \sum_{j \in \mathcal{J}} \tilde{A}_{i,j} I_{PV\_roof,i,j,t} \alpha_{PV\_roof,i,j,t} \tag{14a}$$

$$0 \leq \tilde{A}_{i,j} \leq A_{PV\_roof,max,i,j} b_{i,j} \tag{14b}$$

$$A_{PV\_roof} = \sum_{i \in \mathcal{I}} \sum_{j \in \mathcal{J}} \tilde{A}_{i,j} \tag{14c}$$

$$\sum_{i \in \mathcal{I}} \sum_{j \in \mathcal{J}} b_{i,j} = 1 \tag{14d}$$

The rated capacity of the battery storage $E_{BS,rated}$ is limited by the maximum rated battery storage capacity $E_{BS,max}$. Equation (15a) de-

Table 5
Overview of the five scenarios for grid emissions and export limitations.

Scenario name	Description
S0: Base case	PV installations and a Lithium-ion battery are deployable. Grid GHG emissions at an hourly resolution are based on a marginal approach [6]. PV installation area is limited by the building envelope as described in Table 4. All surplus electricity can be sold to the grid without export limitations.
S1: Constant grid GHG emissions	Grid GHG emission intensity is set to the average annual value (i.e. no hourly or seasonal fluctuations).
S2: Export cap 50%	The electricity export to the grid is limited to 50% of the peak electricity exports in the base case during all hours of operation. Electricity production exceeding the export limit that cannot be stored or used locally is curtailed.
S3: Export cap 25%	The electricity export to the grid is limited to 25% of the peak electricity exports in the base case during all hours of operation. Electricity production exceeding the export limit that cannot be stored or used locally is curtailed.
S4: Export cap 0%	The electricity export to the grid is limited to 0% of peak electricity exports in the base case during all hours of operation. Electricity production exceeding the export limit that cannot be stored or used locally is curtailed.

scribes that the electricity stored at the battery at each time step is the electricity stored at the previous time step plus any electricity that was charged minus any electricity that was discharged. The state of charge of the battery SOC_t must be between the minimum and maximum allowed value (Eq. (15b)). Moreover, the charging power $P_{\mathrm{BS\_in},t}$ and the discharging power $P_{\mathrm{BS\_out},t}$ are limited to a quarter of the rated battery capacity $E_{\mathrm{BS,rated}}$, i.e. the nominal battery capacity in kWh. The duration of one timestep is represented by $\Delta t = 1$ h:

$$E_{BS,rated}\,SOC_t = (1-\lambda_{\mathrm{L}})\,SOC_{t-1}\,E_{\mathrm{BS,rated}} + \eta_{\mathrm{c}}\,P_{\mathrm{BS\_in},t}\,\Delta t - \frac{1}{\eta_{\mathrm{d}}}\,P_{\mathrm{BS\_out},t}\,\Delta t \tag{15a}$$

$$SOC_{\min} \le SOC_t \le SOC_{\max} \tag{15b}$$

$$P_{\mathrm{BS\_out},t} \le \frac{1}{4h}\,E_{\mathrm{BS,rated}} \tag{15c}$$

$$P_{\mathrm{BS\_in},t} \le \frac{1}{4h}\,E_{\mathrm{BS,rated}} \tag{15d}$$

2.2. Energy indicators

To better understand how generated PV electricity is consumed across different scenarios, we use two common energy indicators, namely, self-consumption and self-sufficiency. The self-consumption (SC) indicates how much of the electricity produced on-site is used to satisfy the electricity demand (Eq. (16)):

$$SC = \frac{\sum_{t\in\mathcal{T}}\left(P_{\mathrm{PV\_production},t} - P_{\mathrm{grid\_out},t} - P_{\mathrm{curtailed},t}\right)}{\sum_{t\in\mathcal{T}} P_{\mathrm{PV\_production},t}}\,100 \tag{16}$$

Self-sufficiency (SS), on the other hand, indicates how much of the demand is satisfied by on-site electricity production (Eq. (17)):

$$SS = \frac{\sum_{t\in\mathcal{T}}\left(P_{\mathrm{demand},t} - P_{\mathrm{grid\_in},t}\right)}{\sum_{t\in\mathcal{T}} P_{\mathrm{demand},t}}\,100 \tag{17}$$

The seasonal effects can be analyzed by computing the SC and SS for different parts of the year (e.g. summer and winter half-years).

2.3. Scenarios

Several scenarios are analysed to assess how the results of the cost and emission optimization of the building PV system are influenced by time-resolved grid emissions and export limitations. The scenarios are summarized in Table 5. We assume constant electricity export limits throughout the year, which are defined as a fraction of the peak electricity exports to the grid in the base case scenario. Any electricity production that exceeds the export limit and cannot be stored or used otherwise, must be curtailed. As a result, the potential economic and environmental benefits of exporting electricity to the grid reduce in scenarios where an export limit is applied. In reality, a static export limitation is implemented by controlling the inverter power output based on site's demand to achieve a desired static power output at the feed-in.

Moreover, a sensitivity analysis is included in Appendix B, which examines the role that price and emission assumptions has on our key results. Specifically, a high price scenario and a no-nuclear scenario for the grid GHG emission intensity are examined. Moreover, a scenario combining high prices, no-nuclear grid GHG emission intensity and no electricity exports is also investigated.

3. Results and discussion

3.1. Cost-emission Pareto fronts

The cost-emissions Pareto fronts for the five scenarios (described in Sec. 2.3) are presented in Fig. 3. Most Pareto points perform better both from a cost and an emission perspective than only purchasing electricity from the grid (black) to satisfy the electricity demand. Some minimum cost solutions approach zero, especially in cases where exports are not limited. This indicates that the revenue from sold electricity is close to the sum of the annualized investment costs and the electricity purchased from the grid. Assuming constant GHG grid emissions (yellow) leads to a Pareto front that collapses into one point, as the time at which electricity is exported is irrelevant from an emission perspective. Moreover, Fig. 3 shows that when ignoring the seasonal and hourly fluctuations of the GHG emission intensity of the electric grid, the average emissions per kWh electricity demand are significantly underestimated compared to the minimum cost solution of the base case (blue). In fact, the cost-optimal solution underestimates the GHG emissions significantly when seasonal and hourly fluctuations of the electricity grid are not considered (base case vs constant grid GHG emissions). The constant grid GHG emissions scenario predicts GHG emissions of -30 g_{GHG}/kWh and thus net negative GHG emissions, whereas the same scenario with dynamic grid GHG emissions suggests GHG emissions of 29 g_{GHG}/kWh. Thus, our findings underline the importance of considering dynamic grid GHG emissions when assessing the emissions saving potential of PV and battery systems. The results are sensitive to the assumptions surrounding the embodied emissions of the technologies. Their impact should be examined in future work.

The export cap scenarios allow us to analyze how the optimal solution changes if the grid provider were to enforce constant contractual export limits known at the point of making an installation decision. The solutions in the scenarios where exports are limited (red, purple, and gray) have larger costs and emissions compared to the base case (blue). Export constraints lead to increasing costs at the emission-optimal point compared to simply purchasing electricity from the grid (black). This indicates that combined PV and battery systems might not always be financially beneficial compared to importing electricity from the grid, especially when they are designed and operated with emissions reduction in mind. However, even in the case where no exports are permitted (grey), all solutions yield emissions reductions compared to a scenario where all electricity is imported from the electricity grid, suggesting that installing a PV and battery system will typically result in environmental benefits regardless of the objective function.

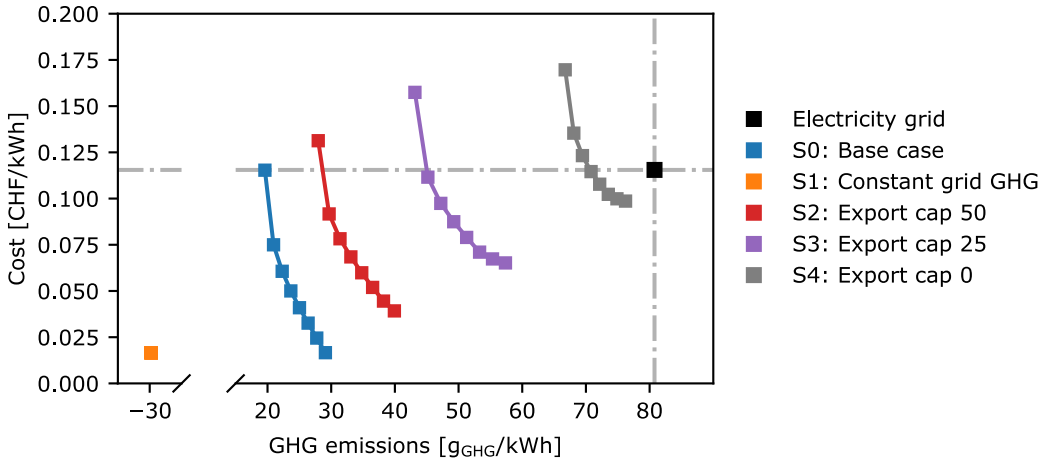

Fig. 3. Pareto fronts for the five considered scenarios: Most solutions improve both system costs and emissions compared to a scenario where the electricity is purely purchased from the grid (black marker). Costs and emissions are normalized by the total demand. For the constant grid GHG emissions case (orange marker) the Pareto front collapses into a single point since the minimum emission and cost point coincide.

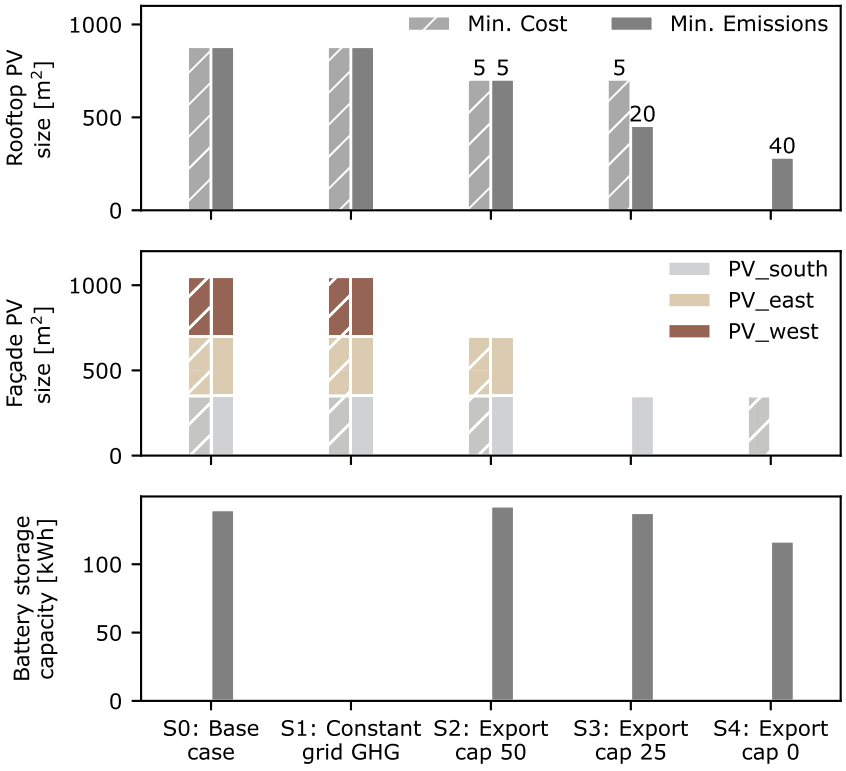

Fig. 4. Sizing of technologies for each scenario at the minimum cost and emission points. Top: rooftop PV installation area with non-zero tilt indicated, ranging between 5 and 40 degrees. In cases of non-zero tilt, the azimuth is slightly shifted east (not shown). Middle: façade PV installations for different orientations. Bottom: Installed battery capacity.

3.2. System design

Fig. 4 illustrates the system design for the cost-optimal solution (left-hand bar, hatched) and the minimum-emission solution (right-hand bar, solid) for the five scenarios S0-S4. The top panel illustrates the installed rooftop PV panel area and the related tilt angles. The middle panel shows the installed façade panel area by orientation. The bottom panel indicates the installed battery capacity in each scenario. The corresponding installation area constraints for the rooftop and façade systems are shown in Table 4. Remarkably, without export limitations (S0-S1), PV installations maximize annual electricity production by fully utilizing the available rooftop area with a 0 degree tilt and maximizing the façade PV installations. These findings are robust to changes in price and grid GHG scenario assumptions, as detailed in Appendix B. Then, with increasing tightness of the export constraints (S2-S4), increasing tilts are observed for both cost- and emission-optimal solutions. Additionally, a decrease in the overall installed façade area can be observed for increasingly strict export limitations, while the battery capacities remain of a similar magnitude as in the base case. The results suggest that, as long as electricity exports are unconstrained, it is more beneficial to maximize the total electricity exports by maximizing the installation area rather than maximizing the plane-of-incidence radiation at the cost of losing the installation area by tilting the PV panels. Additional system design considerations, such as greater susceptibility to soiling for mod-

ules with zero tilt, may eliminate this panel tilt option in the final design stage in favour of slightly higher tilts (e.g. 10 degrees) and/or east-west structures that maximize the active area of the PV modules [60].

The south-facing PV installation, which has the highest plane-of-array irradiance of all the façades, is maximized for emission-optimal solutions unless electricity exports are not allowed (S4). Due to embodied emissions, the south façade is no longer environmentally beneficial at the minimum emission point due to high levels of curtailment throughout the year. However, it is still installed in the cost-optimal solution for S4. The opposite case is observed for S3 with the south façade being installed in the emissions-optimal but not in the cost-optimal solution, indicating that financial and environmental benefits of façade installations must not always coincide. The east façade PV installation is maximised at minimum cost and minimum emissions solutions for S0-S2. The west façade, which has the lowest irradiance per m^2 of all the façades, is only maximized in the minimum cost and emissions solutions for the base (S0) and the constant GHG emissions case (S1).

The installation of batteries further improves the GHG emissions footprint of the solutions by shifting electricity exports to hours with high grid GHG emissions intensities. At the minimum cost point, batteries are not installed for any of the scenarios. Conversely, at the minimum emission point, batteries are installed except for the constant GHG emission case (S1), where shifting electricity exports in time does not yield environmental benefits. When exports are highly constrained (S3-S4), smaller PV installations on a south-facing façade or a rooftop installation with increased tilt are favoured. These installation decisions increase production in the winter half-year due to higher in-plane irradiance compared to flat rooftop systems, as shown in Fig. 2b. When the electricity sold to the grid is limited to 50% of the peak export in the base scenario (S2), the installed battery capacity increases by 1%, while having a 27% smaller PV installation due to no west-facing façade PV installations and a smaller rooftop PV system. Further limiting the allowed electricity exports has a relatively small effect on the installed battery capacities. For example, the installed battery capacity in the export cap 25% scenario (S3) where PV capacity is 57% smaller, the battery capacity is only 1.5% smaller than in the base case (S0). This implies an increased importance of storage (and therefore, self-consumption) when export constraints are placed on surplus generation. Thus, our analysis suggests that with increasingly tight export limitations, smaller PV systems with larger tilts, in combination with south-facing façade PV installations and batteries are optimal from an emissions-perspective.

3.3. GHG emissions abatement from self-consumption and exports

Fig. 5 visualizes the net GHG abatement (dark grey) for each scenario, which includes the GHG abatement due to electricity self-consumption (light grey bars) and electricity exports (light brown bars), minus the systems embodied GHG emissions (red bars). For most scenarios, abatement from electricity exports (via GHG emissions credits) is greater than the abatement due to self-consumption (via a reduction of GHG emissions associated with electricity imports). The abatement from electricity exports is of a similar magnitude as the embodied emissions for scenarios with dynamic GHG emissions. However, our analysis suggests that by using constant grid GHG emissions, GHG emissions abatement is overestimated by a factor of 2 in the cost-optimal case, where system designs are equivalent for S0 and S1. Without any export constraints, both cost- and emission-optimal solutions favour large PV installations with high shares of surplus generation relative to self-consumption (see Fig. 4) and, thus, create environmental benefits via the export of excess electricity production. Thus, in the base case, the abatement from exports exceeds the abatement from increased self-consumption by a factor of 3.3 and 2.1 for the cost- and emissions-optimal solution, respectively. However, in the scenarios with export limitations, the ability to generate environmental benefits via exports is increasingly limited. Thus, environmental benefits from self-consumption play a relatively larger role here. For example, for an export cap of 25% (S3), the ratio from abatement from exports to abatement from increased self-consumption drops to 1.3 and 0.87 for the cost- and emissions-optimal solution, respectively. The higher share of self-consumption is achieved through smaller installed PV systems, large batteries, and, for tighter export constraints, also increasingly tilted rooftop PV systems (see Fig. 4). Consequently, even though the overall GHG emissions abatement potential with a 0% export cap is much smaller at the minimum emission case compared to the base scenario, it presents the only case where GHG emissions abatement from self-consumption exceeds the embodied GHG emissions of the installation, thus allowing for net carbon abatement also without GHG emission credits.

3.4. Self-sufficiency, self-consumption, and curtailed electricity

Fig. 6 shows self-consumption and self-sufficiency across scenarios and curtailed electricity for the scenarios in which electricity exports are constrained, for both the summer and winter half-year. Self-consumption is always higher at the minimum emission point due to the inclusion of a battery system. Export limits significantly increase the self-consumption rate, especially during the more GHG emissions-intense winter half-year. However, while self-consumption increases with increasingly strict export limits, self-sufficiency does not increase, thus suggesting that export limitations might not necessarily foster self-sufficient systems. For example, if electricity exports are completely prohibited (S4), self-consumption of the minimum cost solutions are far from 100% due to high curtailment levels of up to 28%. The trend towards lower self-sufficiency with increasingly strict export limitations is due to lower generation from smaller PV installations. Smaller installations compensate for the loss of export benefits by reducing system-embodied emissions. Generally, comparable or higher self-sufficiency values are observed at the minimum emission point in the winter half-year when compared to the minimum cost point. There is a clear trend towards higher levels of curtailed electricity with tighter electricity export constraints, which are generally higher at the minimum cost point due to the lack of a battery.

4. Conclusion

In this study, we have devised a methodology to assess the optimal orientation and area of photovoltaic (PV) systems, along with determining the optimal capacity of battery storage at the building level considering cost and emissions objectives. Our approach considers dynamic grid GHG emission intensity data and the potential impact of export limitations on installation decisions. Additionally, the model takes into account area-dependent PV system cost estimation, temperature effects on PV efficiency, technology differences between rooftop and façade PV panels, and embodied GHG emissions of PV and battery systems. The environmental and financial benefits of exporting excess electricity production are considered via GHG emissions credits and financial reimbursement for exported electricity, respectively. The environmental and financial benefits from self-consumption are considered via reduced emissions and costs from importing electricity.

The methodology is applied to a mixed-use case study building under different scenarios assessing how constant grid GHG emissions assumptions and export limitations impact system design and operation, while minimizing both costs and emissions. The scenarios are assessed based on resulting installation decisions (i.e. PV area and placement, as well as battery capacity), their corresponding GHG emissions abatement potential (from self-consumption and electricity exports), as well as utilization levels of PV generated electricity (self-consumption, self-sufficiency, and, when relevant, curtailed electricity). Based on the case study results, we draw the following key conclusions:

- Assuming constant grid GHG emission intensity may significantly overestimate the environmental benefits of PV generation. For ex-

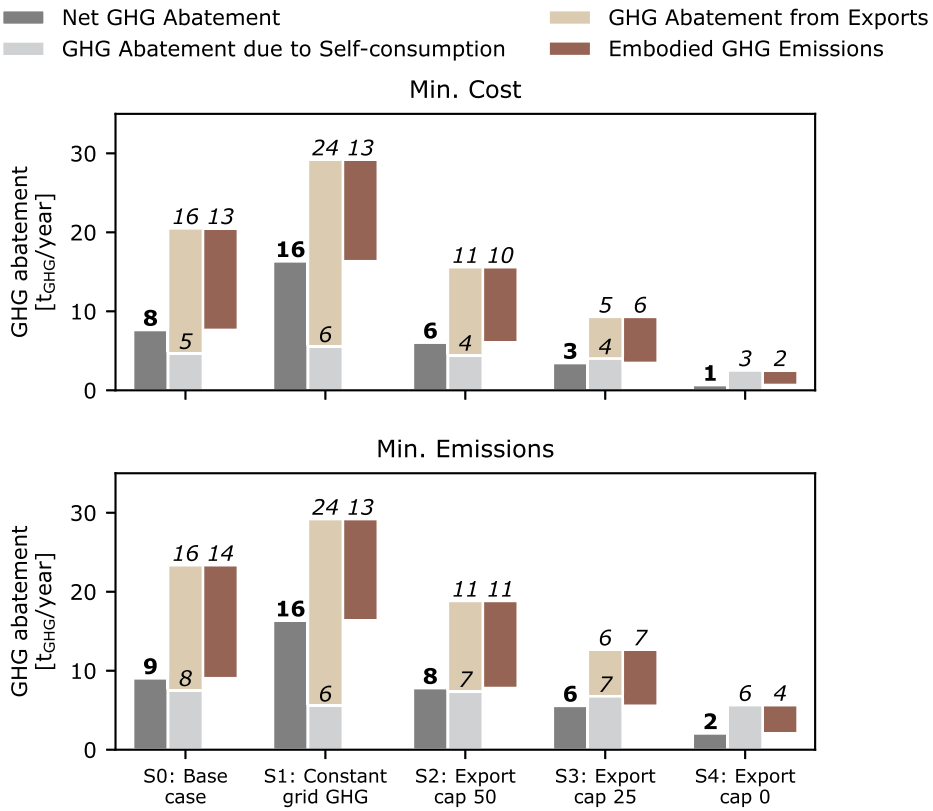

Fig. 5. Scenario-dependent net greenhouse gas (GHG) emissions abatement are shown as the dark grey bars. The GHG emission abatement includes emission savings due to self-consumption (light gray bars) and electricity exports (light brown bars), but reduces due to the system's embodied GHG emissions (red bars).

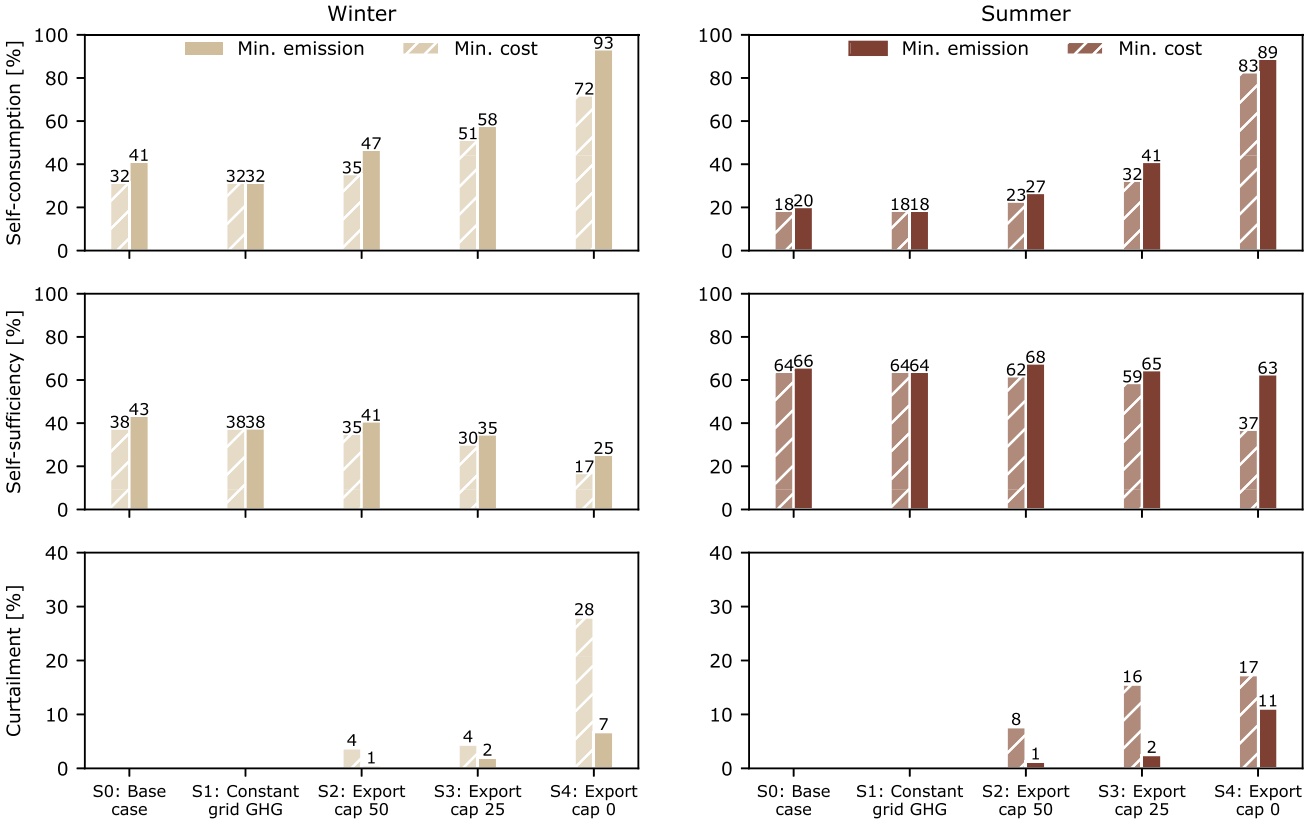

Fig. 6. Overview of self-consumption (top), self-sufficiency (middle) and curtailed electricity (bottom) for summer (Apr-Sept) and winter (Oct-Mar) half-years, on the right and left-hand side, respectively.

ample, the cost-optimal solution without export limitations predicts net negative emissions of 30 $_{GHG}$/kWh for constant grid GHG emissions but positive emissions of 29 $_{GHG}$/kWh when dynamic grid GHG emissions are considered. Consequently, the annual net GHG emissions abatement potential compared to importing electricity from the grid is overestimated by a factor of 2 when neglecting dynamic grid GHG emissions, although the corresponding installation decisions and embodied emissions are equivalent. Moreover, when neglecting dynamic grid GHG emissions, no battery system is installed in the cost- or emissions-optimal case, since there is no environmental benefit from shifting electricity exports in time due to the constant grid GHG emissions.

- When time-resolved grid GHG emissions are considered, large PV installations with high shares of excess electricity production appear beneficial from an environmental and economic perspective for a system with no export limitations (base scenario). A breakdown of environmental benefits reveals that excess electricity production, which is exported and thus credited with emission offsets, is the main contributor to the building's annual GHG emission abatement potential during operation. In the base scenario, GHG emissions abatement from exports is 3.3 times higher than GHG emission abatement from self-consumption at the cost-optimal point. At the emission-optimal point, the breakdown is more balanced, but still in favour of exports by a factor of 2.1. Introducing export limitations shifts this ratio in favour of abatement due to self-consumption, but also lowers overall GHG emissions abatement.
- Electricity export limitations reduce the environmental and financial benefits of excess electricity production, and favour small installations and increased panel tilt. Moreover, the battery capacity remains relatively constant despite the smaller PV panel area for increasingly tight export limitations. Thus, export limitations foster systems with high self-consumption. However, due to smaller PV systems and higher curtailment, export limitations do not foster self-sufficient system, with the self-sufficiency staying relatively constant or even decreasing for stricter export limitations. Self-consumption and self-sufficiency tend to be slightly higher for emissions-optimal solutions compared to cost-optimal solutions, with curtailment being reduced significantly due to battery storage.
- None of the cost-optimal solutions include a battery system. Instead, for tighter electricity export limits, tilted rooftop and/or vertical façade PV systems are observed, which lead to a shift in the times of electricity production. This suggests that further improvements in battery lifetimes and costs are needed to make such investments profitable for consumers. Moreover, this finding emphasizes that when export limitations become more common in the future, consumers should consider installing smaller tilted rooftop and/or vertical façade PV panels for economic reasons.
- Our analysis identifies trade-offs between minimum-emission and minimum-cost system designs. Minimum-emission designs increase self-consumption via the installation of batteries. Aside from addition of batteries, PV system design appears unaffected between cost- and emission-optimal solutions for the base, constant GHG emissions, and the 50% export cap scenarios (S0-S2); under tighter export limits (S3-S4), PV system designs feature different combinations of tilted rooftop and vertical south-facing façade, while maintaining similar installation areas. Cost-optimal designs, on the other hand, favour PV systems without additional storage relying instead on profitable electricity exports.

Our results emphasize the significance of factoring in high-resolution grid GHG emission intensity, export constraints, and angle-dependent PV generation in system design. This approach allows for a more accurate evaluation of the economic and environmental benefits of PV systems during operation, and the impact they have on optimal system design. The trade-offs between cost-effective and emissions-reducing solutions highlight the necessity of aligning these aspects to support decarbonization goals. While the case study's results are specific to the site, our methodology is adaptable to broader applications.

Code and data statement

The code and input data to reproduce the results presented in this work are available on Zenodo: https://doi.org/10.5281/zenodo.10374622.

CRediT authorship contribution statement

Linda Brodnicke: Writing – original draft, Visualization, Validation, Methodology, Formal analysis, Conceptualization. **Alissa Ganter:** Writing – original draft, Visualization, Validation, Methodology, Formal analysis, Conceptualization. **Sven Tröber:** Writing – original draft, Methodology, Investigation, Formal analysis, Data curation. **Giovanni Sansavini:** Writing – review & editing, Supervision. **Natasa Vulic:** Writing – review & editing, Supervision, Conceptualization, Project administration, Writing – original draft.

Declaration of competing interest

The authors declare the following financial interests/personal relationships which may be considered as potential competing interests: Sven Troeber reports a relationship with Green Energy Venture AG that includes: employment. Sven Troeber reports a relationship with Terra Custos AG that includes: board membership. If there are other authors, they declare that they have no known competing financial interests or personal relationships that could have appeared to influence the work reported in this paper.

Data availability

We have shared our data and code on Zenodo.

Acknowledgements

We would like to thank Hanmin Cai and Varsha Behrunani from Empa for assistance with NEST data, Paolo Gabrielli from ETH Zurich for assisting in the formulation of the optimization problem, and Elliot Romano from University of Geneva for providing data on time-resolved grid GHG emission intensity of the Swiss electricity grid. Martin Rüdisüli and Kristina Orehounig are acknowledged for helpful discussion. This project has received funding from the European Union's Horizon 2020 research and innovation programme under the Marie Sklodowska-Curie (MSC) grant agreement No. 847585 - RESPONSE and the Swiss Federal Office of Energy as part of the SWEET PATHFNDR project under the grant agreement SI/502259.

Appendix A. Input data

A.1. Data pre-processing

All electricity, heating and cooling demand data is obtained from the NEST building in Dübendorf for the year 2018 with a 15 minute time resolution. Preprocessing is performed to remove faulty data points and fill in the missing values. For both thermal and electricity demand measurements, outliers were identified and removed. Then, missing data points are filled in based on experience values for electricity and based on ambient temperature correlations for thermal demand data. Specifically, missing electricity data from 2018 is filled in by shifting values from 2019, while the corresponding heating and cooling demand data were supplemented by correlating ambient temperature to thermal demands. Afterwards, all data points are resampled to an hourly time resolution. Finally, the thermal data is converted to electricity demands using a

Table A.1
NEST Configuration in the Case Study.

Unit	Type	Floor area m^2	Heating	Thermal demand kWh/year	Electricity demand kWh/year	Total demand kWh/year
Backbone	Office	1'500	HP	32'825	86'989	119'814
Solace	Office	103	HP	2'205	1'600	3'805
sfw	Office	197	HP	4'176	9'023	13'199
UMAR	Residential	155	HP	3'314	1'893	5'207
vw	Residential	130	HP	2'248	3'297	5'545

Table A.2
Piecewise Affine Approximation of PV costs. [33], [34], [35].

Installation	Parameter	Units	Segment 1	Segment 2	Segment 3	Segment 4
Both	$A_{\min,l}, A_{\min,m}$	m^2	0	11	53	105
Both	$A_{\max,l}, A_{\min,m}$	m^2	11	53	105	-
Rooftop	a_l	CHF/m^2	675.45	294.76	190.77	123.19
Rooftop	b_l	CHF	0	4'187.6	9'699.2	16'795.1
Façade	a_m	CHF/m^2	837.27	263.57	93.08	24.58
Façade	b_m	CHF	0	6'310.7	15'346.9	22'538.9

Table A.3
Electricity Pricing Scheme.

Time period	Tariff	Base scenario		High price scenario	
		Import price Rp/kWh	Export price Rp/kWh	Import price Rp/kWh	Export price Rp/kWh
01.10.-31.03.	High	12.56	8.0	27.05	16.0
01.10.-31.03.	Low	11.06	8.0	25.65	16.0
01.04.-30.09.	High	11.96	8.0	26.55	16.0
01.04.-30.09.	Low	10.56	8.0	25.15	16.0

constant coefficient of performance (COP) of 4.0 for heating and 3.0 for cooling demands.

Table A.1 provides an overview of the considered building units, their relative floor areas and annual demands. The office units have a two times higher specific annual electricity consumption (i.e. per m^2). However, electricity needs to satisfy thermal demands are higher for residential units, mainly due to higher hot water usage.

A.2. PV system cost

The rooftop and façade PV system costs are based on the data from EnergieSchweiz Solarrechner [33], and are modelled by a piecewise affine approximation with four segments, as shown in Table A.2. The same segment lengths are used for rooftop and façade PV, i.e. $A_{\min,l} = A_{\min,m}$ and $A_{\max,l} = A_{\max,m}$.

The rooftop investment costs $C_{\text{PV\_roof}}$ and the façade investment costs $C_{\text{PV\_facades},k}$ are thus calculated as a function of the area of the PV panels on the roof $A_{\text{PV\_roof}}$ and on each façade $A_{\text{PV\_facades},k}$:

$$C_{\text{PV\_roof}} = \sum_{l=1}^{4} \left(a_l A_{\text{PV\_roof}} + b_l\right) y_l \tag{A.1a}$$

$$C_{\text{PV\_facades},k} = \sum_{m=1}^{4} \left(a_m A_{\text{PV\_facades},k} + b_m\right) y_{m,k} \quad \forall k \in \mathcal{K} \tag{A.1b}$$

For example, a 10 m^2 rooftop PV system (Segment 1), with the assumed capacity of 200Wp/m^2 will have a specific system cost of 675 CHF/m^2 or 3.38 CHF/Wp. On the other hand, a 110 m^2 rooftop PV system (Segment 4), will have a specific system cost of 275 CHF/m^2 or 1.38 CHF/Wp (nearly 2.5 lower).

The binary variables y_l and $y_{m,k}$ ensure that the correct segment is selected:

$$\sum_{l=1}^{4} \left(y_l A_{\min,l}\right) \le A_{\text{PV\_roof}} \le \sum_{l=1}^{4} \left(y_l A_{\max,l}\right) \tag{A.2a}$$

$$\sum_{m=1}^{4} \left(y_{m,k} A_{\min,m}\right) \le A_{\text{PV\_facades},k} \le \sum_{m=1}^{4} \left(y_{m,k} A_{\max,m}\right) \quad \forall k \in \mathcal{K} \tag{A.2b}$$

Moreover, at most one segment can be selected:

$$\sum_{l=1}^{4} y_l \le 1 \tag{A.3a}$$

$$\sum_{m=1}^{4} y_{m,k} \le 1 \quad \forall k \in \mathcal{K} \tag{A.3b}$$

A.3. Electricity prices

The following Table A.3 presents the assumed electricity prices. The import prices are the end-user prices for businesses, which include costs for network tariffs, taxes, and levies [51]. The prices depend on the time-of-use, and are higher throughout the day ("high tariff") and lower throughout the night ("low tariff"). Moreover, electricity that is exported is remunerated with the export tariff (FIT), which is also listed in Table A.3. The results in the main body of the manuscript are based on the base scenario price assumptions. In a sensitivity analysis, a high price scenario is examined, and Table A.3 shows the price assumptions. The high price scenario corresponds to 2024 prices and FIT values.

Appendix B. Sensitivity analysis

B.1. Scenarios

The scenarios that are included in the sensitivity analysis are described in Table B.1.

B.2. Pareto front

Fig. B.1 visualizes the Pareto fronts for the base scenario S0, the no export scenario S4, and the sensitivity scenarios S5-S7, described in

Table B.1
Overview of the two scenarios that are included in the sensitivity analysis.

Scenario name	Description
S5: High Price	Same assumptions as for the base case but with import and export prices from 2024, which are significantly higher. The assumed prices are detailed in appendix A.3.
S6: No Nuclear	Same assumptions as for the base case but grid GHG emission intensity uses the marginal emissions by [6] without the presence of nuclear power.
S7: High price, no nuclear, export cap 0	Combination of the high-price scenario, the no-nuclear GHG emission intensity, and without system exports.

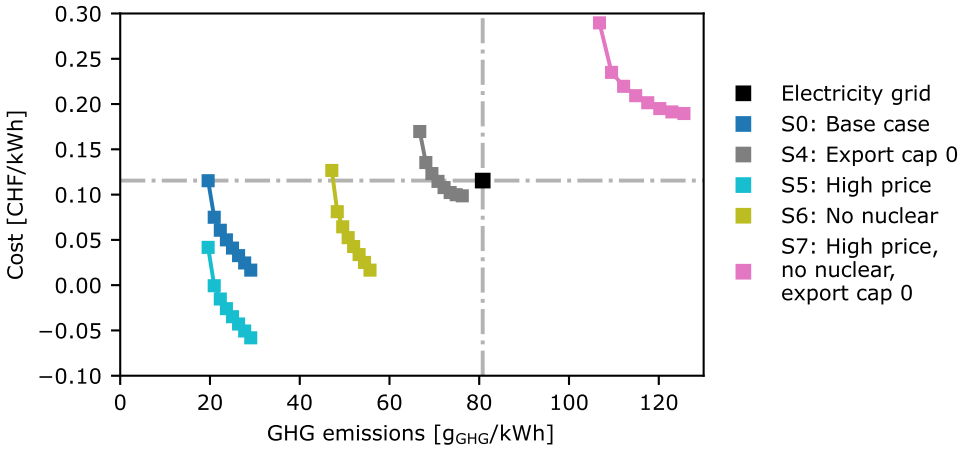

Fig. B.1. Cost-emission Pareto fronts for the sensitivity scenarios S5-S7 in comparison to the base scenario S0 and the no-exports scenario S4. Moreover, the system performance for electricity imports from the grid is illustrated for the price and emissions assumptions of the base case.

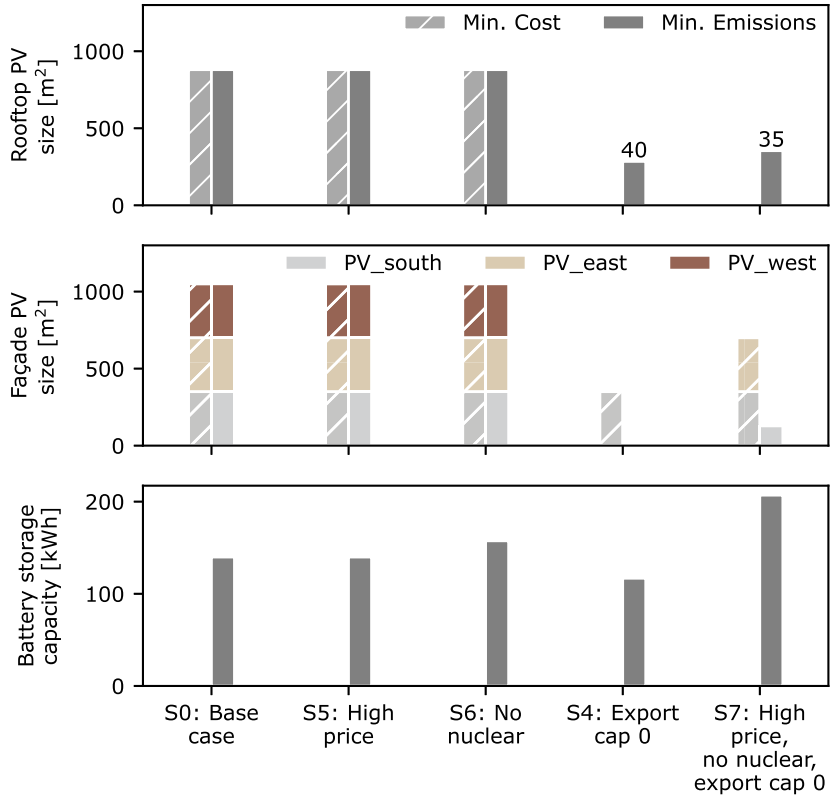

Fig. B.2. Sizing of technologies for the sensitivity scenarios S5-S7 at the minimum cost and emission points in comparison to the base scenario S0 and the no-export scenario S4. Top: rooftop PV installation area with non-zero tilt indicated. Middle: façade PV installations for different orientations. Bottom: Installed battery capacity.

Sec. Appendix B.1. In the high price scenario, where import and export prices from 2024 are considered, GHG emission values remain the same, while costs are reduced by about 0.08 CHF/kWh. With the exception of the minimum-emission solution, revenues (negative costs) are generated due to the increased profitability of exports due to the doubling of the feed-in tariff. In scenario S6, where nuclear power is not present in the mix of the electricity grid, GHG emission values increase by a factor of 1.9-2.4 compared to the base scenario S0. Furthermore,

the minimum-cost values of scenarios S0 and S6 coincide. However, as GHG emissions reduce, costs increase between 2%-10% compared to the base scenario S0. When considering high prices, the no-nuclear GHG emission intensity, and no permitted exports (S7), a significant increase in both costs and emissions is visible for all solutions of the Pareto front. This suggests that export limitations increase the effect of higher prices and emissions, since no economic or environmental benefits in form of financial reimbursement and GHG emissions credits can be collected via exports.

B.3. System design

Fig. 4 illustrates the system design for the cost-optimal solution (left-hand bar, hatched) and the minimum-emission solution (right-hand bar, solid) for the base scenario S0 and the no-export scenario S4, and the sensitivity scenarios S5-S7. The system design in scenarios S0 and S5 is identical. However, the higher export prices in scenario S5 result in lower system cost due to the increased profitability of exports (Fig. B.1). Furthermore, we observe identical system designs for the minimum-cost solutions of base scenario S0 and scenario S6. However, due to the phaseout of nuclear power plants, grid GHG emissions are higher in scenario S6 compared to scenario S5. To reduce grid imports and reduce GHG emissions, scenario S6, therefore, installs larger battery storage in the minimum-emission solution (+13% compared to S0). While this increase in battery storage capacity yields lower GHG emissions, system cost increases by 10% compared to the base scenario S0. A comparison of scenarios S4 and S7 reveals that due to the higher GHG emission intensity, a larger battery is installed in the emission-optimal case. This can be explained by a higher emissions intensity of electricity imports making self-consumption more preferable. In the cost-optimal solution, the east-facing façade system becomes cost-efficient due to the higher import prices, thus resulting in a larger overall installed PV system (Fig. B.2).

References

[1] BFE, Was ist die energie strategie 2050?, https://www.bfe.admin.ch/bfe/de/home/politik/energiestrategie-2050/was-ist-die-energiestrategie-2050.html, 2020.

[2] Bundesamt für Energie, Energieperspektiven 2050+, https://www.bfe.admin.ch/bfe/de/home/politik/energieperspektiven-2050-plus.html, 2020.

[3] BFE, Meteoschweiz, swisstopo, Sonnendach-Daten, Tech. Rep., BFE, Meteoschweiz, swisstopo, 2017, https://www.uvek-gis.admin.ch/BFE/sonnendach/.

[4] BFE, BFE, Statistik Sonnenenergie, Tech. Rep., BFE, 2023.

[5] E. Romano, P. Hollmuller, M. Patel, Émissions horaires de gaz à effet de serre liées à la consommation d'électricité – une approche incrémentale pour une économie ouverte: Le cas de la Suisse, Arch. ouverte UNIGE (2018) 25, https://archive-ouverte.unige.ch/unige:131622.

[6] M. Rüdisüli, E. Romano, S. Eggimann, M.K. Patel, Decarbonization strategies for Switzerland considering embedded greenhouse gas emissions in electricity imports, Energy Policy 162 (2022) 112794, https://doi.org/10.1016/j.enpol.2022.112794.

[7] M. Rüdisüli, S.L. Teske, U. Elber, Impacts of an increased substitution of fossil energy carriers with electricity-based technologies on the Swiss electricity system, Energies 12 (12) (2019), https://doi.org/10.3390/en12122399.

[8] N. Lienhard, R. Mutschler, L. Leenders, M. Rüdisüli, Concurrent deficit and surplus situations in the future renewable Swiss and European electricity system, Energy Strategy Rev. 46 (2023) 101036, https://doi.org/10.1016/j.esr.2022.101036.

[9] E. O'Shaughnessy, J.R. Cruce, K. Xu, Too much of a good thing? Global trends in the curtailment of solar PV, Sol. Energy 208 (2020) 1068–1077, https://doi.org/10.1016/j.solener.2020.08.075.

[10] R. Luthander, D. Lingfors, J. Widén, Large-scale integration of photovoltaic power in a distribution grid using power curtailment and energy storage, Sol. Energy 155 (2017) 1319–1325, https://doi.org/10.1016/j.solener.2017.07.083.

[11] M. Perez, R. Perez, K.R. Rábago, M. Putnam, Overbuilding & curtailment: the cost-effective enablers of firm PV generation, Sol. Energy 180 (December 2018) 412–422, https://doi.org/10.1016/j.solener.2018.12.074, 2019.

[12] Bundesanzeiger, Gesetz zur neuregelung des rechtsrahmens für die förderung der stromerzeugung aus erneuerbaren energien, https://www.clearingstelle-eeg-kwkg.de/sites/default/files/BGBl_2011_I_1634.pdf, 2011.

[13] Verband Schweizerischer Elektrizitätsunternehmen, Stellungnahme zur umsetzung der änderung vom 1. oktober 2021 des energie- gesetzes auf verordnungsstufe und weitere änderungen der energieverordnung, der energieeffizienzverordnung, der energieförderungsverordnung und der strom- versorgungsverordnung mit inkrafttreten anfang 2023, https://www.strom.ch/de, 2022.

[14] Australian Energy Regulator, Connection charge guidelines for electricity customers, https://www.aer.gov.au/system/files/AER%20-%20Connection%20charge%20guidelines%20for%20electricity%20customers%20-%20April%202023.pdf, 2023.

[15] G.B. Litjens, E. Worrell, W.G. van Sark, Influence of demand patterns on the optimal orientation of photovoltaic systems, Sol. Energy 155 (2017) 1002–1014, https://doi.org/10.1016/j.solener.2017.07.006.

[16] M. Brito, S. Freitas, S. Guimarães, C. Catita, P. Redweik, The importance of facades for the solar PV potential of a Mediterranean city using LiDAR data, Renew. Energy 111 (2017) 85–94, https://doi.org/10.1016/j.renene.2017.03.085.

[17] I.H. Rowlands, B. Paige, I. Beausoleil-morrison, Optimal solar-PV tilt angle and azimuth: an Ontario (Canada) case-study, Energy Policy 39 (3) (2011) 1397–1409, https://doi.org/10.1016/j.enpol.2010.12.012.

[18] M. Lovati, G. Salvalai, G. Fratus, L. Maturi, R. Albatici, D. Moser, New method for the early design of BIPV with electric storage: a case study in northern Italy, Sustain. Cities Soc. 48 (2019) 101400, https://doi.org/10.1016/j.scs.2018.12.028.

[19] N. Franzoi, A. Prada, S. Verones, P. Baggio, Enhancing PV self-consumption through energy communities in heating-dominated climates, Energies 14 (14) (2021) 4165, https://doi.org/10.3390/en14144165.

[20] S. Freitas, C. Reinhart, M.C. Brito, Minimizing storage needs for large scale photovoltaics in the urban environment, Sol. Energy 159 (2018) 375–389, https://doi.org/10.1016/j.solener.2017.11.011.

[21] J. Weniger, T. Tjaden, V. Quaschning, Sizing of residential PV battery systems, Energy Proc. 46 (2014) 78–87, https://doi.org/10.1016/j.egypro.2014.01.160.

[22] A. Walch, M. Rüdisüli, Strategic PV expansion and its impact on regional electricity self-sufficiency: case study of Switzerland, Appl. Energy 346 (2023) 121262, https://doi.org/10.1016/j.apenergy.2023.121262.

[23] J.A. Azzolini, M.J. Reno, K.A. Horowitz, Evaluation of curtailment associated with PV system design considerations, IEEE Power Energy Soc. Gen. Meet. (2020), https://doi.org/10.1109/pesgm41954.2020.9281427.

[24] B. Matthiss, D. Stellbogen, M. Eberspächer, J. Binder, Curtailed energy of pv systems – dependency on grid loading limit, orientation and local energy demand, in: 31st European Photovoltaic Solar Energy Conference and Exhibition, pp. 2311–2314, https://doi.org/10.4229/EUPVSEC20152015-5BV.2.46.

[25] J.I. Laveyne, D. Bozalakov, G. Van Eetvelde, L. Vandevelde, Impact of solar panel orientation on the integration of solar energy in low-voltage distribution grids, Int. J. Photoenergy 2020 (2020) 1–13, https://doi.org/10.1155/2020/2412780.

[26] C. Waibel, G. Mavromatidis, A. Bollinger, R. Evins, J. Carmeliet, Sensitivity analysis on optimal placement of façade based photovoltaics, in: ECOS 2018 - Proceedings of the 31st International Conference on Efficiency, Cost, Optimization, Simulation and Environmental Impact of Energy Systems, 2018, https://www.dora.lib4ri.ch/empa/islandora/object/empa:22695.

[27] NEST collaboration, https://wiki.nestcloud.ch/bin/view/Main/.

[28] MeteoSchweiz, https://www.meteoschweiz.admin.ch/.

[29] W.F. Holmgren, C.W. Hansen, M.A. Mikofski, Pvlib python: a python package for modeling solar energy systems, J. Open Sour. Softw. 3 (29) (2018) 884, https://doi.org/10.21105/joss.00884.

[30] S. Diamond, S. Boyd, CVXPY: a python-embedded modeling language for convex optimization, J. Mach. Learn. Res. 17 (83) (2016) 1–5, http://jmlr.org/papers/v17/15-408.html.

[31] A. Agrawal, R. Verschueren, S. Diamond, S. Boyd, A rewriting system for convex optimization problems, J. Control Decis. 5 (1) (2018) 42–60, https://doi.org/10.1080/23307706.2017.1397554.

[32] Gurobi Optimization, LCC, Gurobi Optimizer Reference Manual, https://www.gurobi.com/documentation/current/refman/index.html, 2022.

[33] Solarrechner: Kosten- und nutzenrechner für ihre solaranlage, https://www.energieschweiz.ch/tools/solarrechner/.

[34] Bundesamt für Energie, P+D-Projekt: BIPV-Fassaden Benchmark (November), https://www.aramis.admin.ch/Default?DocumentID=66824&Load=true, 2020.

[35] H. Gholami, H.N. Røstvik, Economic analysis of BIPV systems as a building envelope material for building skins in Europe, Energy 204 (2020) 117931, https://doi.org/10.1016/j.energy.2020.117931.

[36] Fraunhofer, Photovoltaics report, https://www.ise.fraunhofer.de/en/publications/studies/photovoltaics-report.html.

[37] PVSyst, Array thermal losses, https://www.pvsyst.com/help/index.html?thermal_loss.html, 2023.

[38] A. Virtuani, D. Pavanello, G. Friesen, Overview of temperature coefficients of different thin film photovoltaic technologies, in: 25th European Photovoltaic Solar Energy Conference and Exhibition / 5th World Conference on Photovoltaic Energy Conversion 6-10 September 2010, 2010, 5 pages, 781 kb https://userarea.eupvsec.org/proceedings/25th-EU-PVSEC-WCPEC-5/4AV.3.83/.

[39] R. Frischknecht, P. Stolz, L. Krebs, M. de Wild-Scholten, P. Sinha, V. Fthenakis, C. Kim, M. Raugei, M. Stucki, Life Cycle Inventories and Life Cycle Assessments of Photovoltaic Systems 2020, Tech. Rep., IEA, 2020, https://iea-pvps.org/wp-content/uploads/2020/12/IEA-PVPS-LCI-report-2020.pdf.

[40] R. Frischknecht, L. Krebs, Ökobilanz Strom aus Photovoltaikanlagen Update 2020 - Factsheet, v1.0 (2020) 1–17.

[41] Meyer burger glass 370-390 wp, https://www.meyerburger.com/en/solar-products-for-private-use.

[42] aesolar product catalog, https://ae-solar.com/products-list/.
[43] Tesla, Powerwall 2 Datasheet, Switzerland, 2019.
[44] M. Chordia, A. Nordelöf, L.A.W. Ellingsen, Environmental life cycle implications of upscaling lithium-ion battery production, Int J. Life-Cycle Assess. (2021), https://doi.org/10.1007/s11367-021-01976-0, (Strauch 2020).
[45] L. Lu, X. Han, J. Li, J. Hua, M. Ouyang, A review on the key issues for lithium-ion battery management in electric vehicles, J. Power Sources 226 (2013) 272–288, https://doi.org/10.1016/j.jpowsour.2012.10.060.
[46] N. Kularatna, Rechargeable batteries and their management, IEEE Instrum. Meas. Mag. 14 (2) (2011) 20–33, https://doi.org/10.1109/MIM.2011.5735252.
[47] D. Dallinger, J. Link, M. Büttner, Smart grid agent: plug-in electric vehicle, IEEE Trans. Sustain. Energy 5 (3) (2014) 710–717, https://doi.org/10.1109/TSTE.2014.2298887.
[48] M. Ecker, N. Nieto, S. Käbitz, J. Schmalstieg, H. Blanke, A. Warnecke, D.U. Sauer, Calendar and cycle life study of li(nimnco)o2-based 18650 lithium-ion batteries, J. Power Sources 248 (2014) 839–851, https://doi.org/10.1016/j.jpowsour.2013.09.143.
[49] S. Odeh, T.H. Nguyen, Assessment method to identify the potential of rooftop PV systems in the residential districts, Energies 14 (14) (2021) 1–11, https://doi.org/10.3390/en14144240.
[50] D. Wang, J. Landolt, G. Mavromatidis, K. Orehounig, J. Carmeliet, CESAR: a bottom-up building stock modelling tool for Switzerland to address sustainable energy transformation strategies, Energy Build. 169 (2018) 9–26, https://doi.org/10.1016/j.enbuild.2018.03.020.
[51] Downloads Glattwerk AG, https://www.glattwerk.ch/downloads.
[52] R. Perez, R. Seals, P. Ineichen, R. Stewart, D. Menicucci, A new simplified version of the Perez diffuse irradiance model for tilted surfaces, Sol. Energy 39 (3) (1987) 221–231, https://doi.org/10.1016/S0038-092X(87)80031-2.
[53] R. Perez, P. Ineichen, R. Seals, J. Michalsky, R. Stewart, Modeling daylight availability and irradiance components from direct and global irradiance, Sol. Energy 44 (5) (1990) 271–289, https://doi.org/10.1016/0038-092X(90)90055-H.
[54] K. Kawajiri, T. Oozeki, Y. Genchi, Effect of temperature on PV potential in the world, Environ. Sci. Technol. 45 (20) (2011) 9030–9035, https://doi.org/10.1021/es200635x, publisher: American Chemical Society.
[55] A. Driesse, M. Theristis, J.S. Stein, Pv module operating temperature model equivalence and parameter translation, in: 2022 IEEE 49th Photovoltaics Specialists Conference (PVSC), 2022, pp. 0172–0177.
[56] pvlib, PV temperature models, https://pvlib-python.readthedocs.io/en/stable/reference/pv_modeling/temperature.html, 2023.
[57] pvlib, pvlib.temperature pvsyst_cell, https://pvlib-python.readthedocs.io/en/stable/reference/generated/pvlib.temperature.pvsyst_cell.html, 2023.
[58] A. Dobos, PVWatts version 5 manual, https://pvwatts.nrel.gov/downloads/pvwattsv5.pdf, 2014.
[59] G. Mavrotas, Effective implementation of the epsilon-constraint method in multi-objective mathematical programming problems, Appl. Math. Comput. 213 (2) (2009) 455–465, https://doi.org/10.1016/j.amc.2009.03.037.
[60] S.P. World, East-West solar projects maximize the number of panels on an array, https://www.solarpowerworldonline.com/2021/12/east-west-solar-projects-maximize-the-number-of-solar-panels-on-an-array/.